IEEE Access
Multidisciplinary | Rapid Review | Open Access Journal

Received November 5, 2021, accepted November 10, 2021, date of publication November 16, 2021,
date of current version December 10, 2021.

Digital Object Identifier 10.1109/ACCESS.2021.3128398

Best Input–Location Pair Selection for SSR Damping Controller in DFIG Based Wind Farms

S. R. JAYAKRISHNAN, ELIZABETH P. CHERIYAN, (Senior Member, IEEE), AND T. K. SINDHU, (Member, IEEE)
Department of Electrical Engineering, National Institute of Technology Calicut, Kozhikode, Kerala 673601, India
Corresponding author: S. R. Jayakrishnan (jayakrishnan_p140089ee@nitc.ac.in)

ABSTRACT Mitigation of Sub-Synchronous Resonance (SSR) in Doubly-Fed Induction Generator (DFIG) based wind farms by incorporating a Supplementary Damping Controller (SDC) to the existing DFIG converter controllers is more economical than providing additional FACTS devices to the system. The performance of the SDC highly depends on its location and the Input Control Signal (ICS) selected. Hence, a systematic method for selecting the best ICS- location pair for SDC is the need of the hour. Hence in this paper, a technique to identify the best ICS- location pair for SDC based on the right half-plane zero method, relative gain array method, and Henkel singular value is proposed. The performance of the proposed strategy is then compared with that of the generally used residue-based selection method and joint geometric controllability method. A proportional feedback controller based on the root locus method is designed to validate the results of the proposed method. Extensive simulation studies using MATLAB/Simulink are carried out to evaluate the performance of the proposed method.

INDEX TERMS Doubly-fed induction generator (DFIG), sub-synchronous resonance (SSR), supplementary damping controller (SDC), input signal selection, optimal location for damping controller.

I. INTRODUCTION

The growth of wind power technology is tremendous, and the integration of large scale wind energy into the grid has become more critical. This requires the up-gradation of transmission line infrastructure to keep pace with wind power generation. DFIG based techniques are most commonly used in wind generation due to the capability of power system damping control for improving rotor angle stability, providing flexible voltage and active power control. In addition, DFIG also provides low cost, smaller size, improved efficiency, and mechanical stress reduction [1], [2]. The studies presented in [3] and the references therein have shown that series compensation is the cost-effective solution to improve the power transfer capability and reliability of an existing transmission system rather than constructing new transmission lines. However, one of the major factors deterring the extensive usage of capacitive compensation with capacitor banks is the potential risk of Sub-Synchronous Oscillation (SSO) due to electromechanical interactions of DFIG shaft system with other power system components [4].

The associate editor coordinating the review of this manuscript and approving it for publication was Nagesh Prabhu.

SSO is a condition in which a wind farm exchanges energy with the electrical network at one or more natural frequencies of the power system [5]. SSO is classified into Sub-Synchronous Resonance (SSR), Sub-Synchronous Torsional Interaction (SSTI), and Sub-Synchronous Control Interaction (SSCI) [6], [7]. Due to the series resonance effect of line reactance and series capacitance under disturbance conditions, the net resistance corresponding to the subsynchronous current seen from the wind generator is negative. This would result in the overshoot of generator stator voltage, known as Induction Generator Effect (IGE) [8]. Sometimes, the natural frequency of the mechanical systems come close to the natural frequencies of electrical systems, which undams mechanical oscillations. This phenomenon is due to Torsional Interaction (TI) [9], [10]. During transient conditions, generator torque in the subsynchronous frequency range may be induced in the DFIG rotor, which tends to amplify rapidly and cause severe mechanical damage to the wind turbine. This phenomenon is known as Torsional Amplification (TA). Compared to IGE and TI, TA is a fast and severe phenomenon [11], [12]. The impact of SSCI on DFIG based wind farms and the influence of DFIG converter controller parameters on SSCI have been studied extensively using

Electro-Magnetic Transient (EMT) analysis in [13]. Since the scope of this work is limited to the study of SSR analysis only, the study of damping controller parameters changes on SSCI oscillations is suggested as future work. The proposed work addresses the SSR and the mitigation of the same in DFIG based wind farms.

If the development of SSR is not mitigated effectively, the oscillation will leads to equipment damage, loss of power generation, power quality issues, and loss of reliability of the wind power system [2], [14]. The SSR mitigation techniques investigated in the literature can be classified into two broad categories. In the first approach, FACTS devices such as STATCOM [4], [15], TCSC [3], [16], SVC [16], UPFC [17], [18], SSSC [4], [19] and GCSC [20] are employed for SSR mitigation. However, the installation of FACTS devices in the power system is not an economical solution. Thus in the second approach, a Supplementary Damping Controller (SDC) is added to the existing DFIG converter controllers, Grid Side Converter (GSC) and Rotor Side Converter (RSC) [21]–[23]. A nonlinear controller based on state feedback linearization is explained in [24] to mitigate SSCI in DFIG based wind farms. In contrast, a combined control strategy based on feedback linearization control and sliding mode control is presented in [25] and [26] for mitigating SSCI in DFIG based wind farms. [27] Discussed energy-shaping-based controllers for mitigating SSCI in DFIG-based wind farms, while [28] proposed energy-shaping controllers based on the Hamiltonian model for mitigating SSCI in Permanent Magnetic Synchronous Generator (PMSG). A linear proportional feedback controller is used for mitigating SSR in DFIG based wind farms in [29]. The linear proportional controller is relatively simple and easy to design. The proportional feedback controller has a fast response, smaller steady-state error, and dynamically, it is relatively stable [30]. On the other hand, nonlinear controllers are more complex in design [31], [32]. But due to the improved robustness of the system under external disturbances and parameter uncertainties, nonlinear controllers are preferred over linear controllers for damping SSR in DFIG based wind farms [25].

The performance of the SDC highly depends on its Input Control Signal (ICS) - location selection, since combined controllability and observability plays a critical role in damping performance [33], [34]. A systematic and quantitative method to identify the best location of SDC in DFIG is explained in [35]. Location dependent performance index is defined and is used to identify the best location for SDC. However, a systematic selection method for ICS is not explored in the paper. Rotor speed is considered as ICS in [36], and GSC outer control loop is chosen as the location for adding SDC. Performance of damping controllers based on line current and line power is studied in [37], outer control loop of GSC controller is considered as the preferred location for placing SDC. The selection of ICS and location for SDC are arbitrary in [36] and [37].The voltage across the series capacitor is chosen as ICS based on residue analysis in [3], and the GSC outer control loop is chosen as the location for SDC. In [38], both GSC and RSC converter controllers are used as the location for placing SDC, and on the comparison, it is found that RSC controllers have better damping performances. Based on arbitrary selection, the DFIG stator current is used as the ICS in this work. All the eight possible locations for placing SDC in GSC and RSC converter controllers were explored in [20] and [29]. Rotor speed, transmission line power, the voltage across capacitor and transmission line current are used as ICS. Moreover, the best ICS- location pair was chosen based on residue analysis. In [3], the GSC outer converter control loop is considered as the location for SDC; rotor speed, the voltage across the capacitor, transmission line current and DFIG stator voltage are used as ICS. Based on the results of the residue analysis, it is determined that the voltage across the capacitor is the best suitable ICS. Most of the SSR mitigation techniques discussed in the literature use a random selection of ICS and location for SDC. However in [3], [20], [29] residue method technique is used for ICS selection. Since in residue analysis, the behaviour of only one mode is considered at a time, the performance of SDC affects the stability of other modes [33]. In addition to that, if the available input signals for selection have different units, the selection based on the residue method may not be accurate since the residues depend on the scale of the input signals [39]. In [40], [41], and [42] Joint Geometric Controllability and Observability Measures (JGCOM) were used to identify the best control signal and location for damping controllers in the power system. The comparison of the proposed method with joint geometric controllability based selection is also included in this work. However, in this literature, a single criteria based selection approach is adopted, and it does not consider the suitability of selection based on decentralised control application. Hence the observations from the literature survey can be summarised as;

- The most economical method for damping SSR in DFIG based wind farms is by means of introducing SDC to the existing DFIG converter controllers [21]–[23].
- There are eight possible locations available in the DFIG converter controllers, four from GSC and four from RSC, to place SDC. Many options such as DFIG stator voltage, the voltage across the capacitor, transmission line current, line power and rotor speed are available as ICS [3], [20], [29].
- The combined selection of location and ICS for SDC is critical in SSR damping [33], [34].
- The most commonly used method for the selection of best ICS- location pair is residue-based analysis, which is not reliable due to the limitations mentioned [33], [39].
- Since the main focus of the work is to develop a systematic procedure for selecting the best input-location pair SSRDC to mitigate SSR in DFIG based wind farms, a simple and basic linear proportional feedback controller is designed to validate the proposed procedure.

Incorporation of DFIG converter controllers for damping SSR in DFIG based wind farms is more economical than

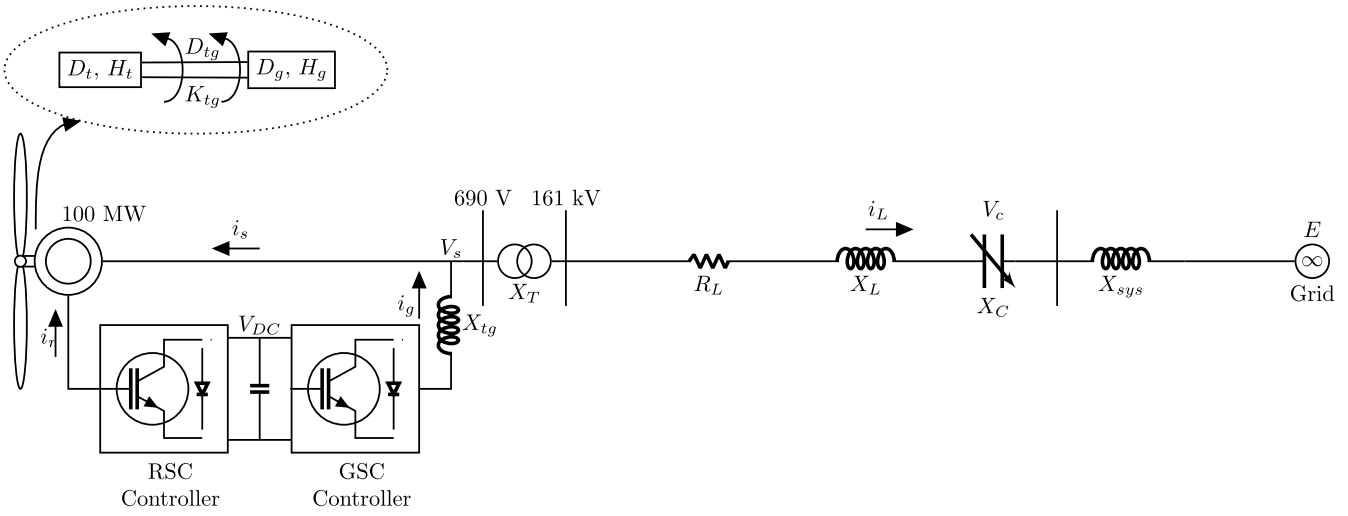

FIGURE 1. DFIG based wind farm connected to grid through series compensated transmission line.

additional FACTs devices. The performance of the damping controller highly depends on the input control signal selected and the location of SDC. Hence a systematic procedure for selecting the best ICS-location pair for SDC to damp SSR in DFIG based wind farms is the need of the hour. However, to the best of our knowledge, no research in the existing literature addresses this problem. So the main contribution of this paper is to propose a new selection procedure to identify the best ICS – location combination for SDC to damp SSR in DFIG based wind farms. In the proposed method, Right Half Plane Zero (RHPZ) [30], Relative Gain Array (RGA) [30], [43] and Henkel Singular Value (HSV) [30], [39], [44] methods have been used in a systematic way to decide the best ICS-location pair.

The main objectives of this paper are listed below.

- A novel procedure for selecting the best ICS-location combinations for designing SDC for damping SSR in DFIG based wind farms is proposed.
- The performance of the proposed method is validated by designing a proportional feedback controller based on the root locus method.
- Time-domain simulations of the study system using MATLAB/Simulink are conducted with SDC designed based on the proposed method's observations.
- SSR possibilities in DFIG based wind farms connected to the grid through series compensated transmission line are analysed.

The rest of the paper is organised as follows. Section II discusses the small signal stability analysis for identifying the SSR possibilities. The procedure for selecting the best ICS-location pair is detailed in Sections III and IV. Validation of the proposed method using time-domain simulation and comparison of the proposed method with residue analysis-based and joint geometric controllability and observability based selection techniques are discussed in section V. Finally, the paper concludes with Section VI.

II. SMALL SIGNAL ANALYSIS FOR IDENTIFYING SSR POSSIBILITIES

The SSR studies on DFIG based wind farms are conducted using small-signal analysis tools such as Eigen-Value Analysis (EVA) by linearising the nonlinear dynamic model of the system around an equilibrium point [45]. Since the complete mathematical model is used in EVA, the method can be used to analyse IGE, and TI [3], [46]. Moreover, EVA provides the details of the frequency and damping of each mode in a single calculation. The effect of parameter variations can also be examined using EVA. Due to these vivid advantages, EVA is widely accepted for SSR analysis [45].

A. SYSTEM USED FOR STUDY

A system consisting of 50 number of 2MW DFIG wind generators connected to the grid through series compensated transmission line is shown in Fig 1. This system model is adopted from the IEEE first benchmark model used for SSR analysis [47], [48]. Researches support the assumption of considering an aggregated model of 100MW model instead of 50 numbers of 2MW generators [49], [50]. In [50], an aggregate model of the wind farm based on DFIG wind turbines was proposed to conduct extensive power system studies instead of a detailed model of the wind farms.

The significant assumptions made in the work are,

- The rated power of the aggregated model is equal to the sum of all individual wind turbines.
- All the wind turbines are experiencing the equivalent average wind; therefore, the generated mechanical torque will be the same for all turbines.
- Control schemes, controller parameters, and protection systems are the same for aggregated wind models and individual wind turbines.

The performance of the aggregated system was compared with that of the detailed model using simulation study for various conditions of wind fluctuations and grid disturbances.

Further, it is concluded that aggregated model of wind farms can be used instead of the detailed model if the difference in average wind speed is less than 2m/s [50]. Moreover the same model has been widely used for SSR analysis in DFIG based wind farms [3], [12], [51]. Hence, this study uses the aggregated model of DFIG wind farms instead of a detailed model.

The system consists of a slip ring induction machine, back to back converters, shaft system and series compensated transmission line. The stator of the induction machine is directly connected to the grid while the rotor circuit is connected to the grid through back to back converter. There is a DC bus linking the back to back converters. The two converters are named Rotor Side Converter (RSC), connecting the rotor circuit to the DC bus, and Grid Side Converter (GSC), connecting the DC bus and grid.

B. MODELING OF THE STUDY SYSTEM

In order to conduct EVA, the complete dynamic model of the study system is needed. Various components such as induction machine, back to back converters, DC bus, shaft system and series compensated transmission line are modelled in this section.

1) MODELING OF INDUCTION MACHINE

Dynamic model of induction machine in dq reference frame is considered for analysis [11], [12]. Stator and rotor currents in the dq frame are chosen as state variables and the corresponding voltages as input variables. All the variables and parameters are considered per unit for ease of doing analysis.

$$\dot{X}_{DFIG} = A_{DFIG}X_{DFIG} + B_{DFIG}U_{DFIG} \quad (1)$$

$$X_{DFIG} = [i_{qs}\ \ i_{ds}\ \ i_{qr}\ \ i_{dr}]^T \quad (2)$$

$$U_{DFIG} = [v_{qs}\ \ v_{ds}\ \ v_{qr}\ \ v_{dr}]^T \quad (3)$$

$$B_{DFIG} = \begin{bmatrix} \frac{\omega_b X_{rr}}{X_D} & 0 & \frac{-\omega_b X_m}{X_D} & 0 \\ 0 & \frac{\omega_b X_{rr}}{X_D} & 0 & \frac{-\omega_b X_m}{X_D} \\ \frac{-\omega_b X_m}{X_D} & 0 & \frac{\omega_b X_{ss}}{X_D} & 0 \\ 0 & \frac{-\omega_b X_m}{X_D} & 0 & \frac{\omega_b X_{ss}}{X_D} \end{bmatrix} \quad (5)$$

where $X_D = X_{rr}X_{ss} - X_m^2$.

The i, v and R are currents, voltages and resistance. With subscript d, q representing the direct and quadrature axis components. Stator and rotor parameters are distinguished by subscript s and r. X_m is the magnetizing reactance of the generator, X_{ls} and X_{lr} are stator and rotor leakage reactance. X_{ss} and X_{rr} are stator and rotor reactance. ω_s, ω_m and ω_b denotes rotating synchronous frame frequency, generator rotor speed and base frequency.

2) MODELING OF SHAFT SYSTEM

The shaft system is modelled by considering two mass model of the system [11], [12], which includes high speed generator mass and low speed turbine mass connected by a spring and damper. The motion equation of the two mass system can be represented by three first order equations as,

$$\dot{X}_{Shaft} = A_{Shaft}X_{Shaft} + B_{Shaft}U_{Shaft} \quad (6)$$

$$X_{Shaft} = [\bar{\omega}_m\ \ \bar{\omega}_r\ \ T_{tg}]^T \quad (7)$$

$$U_{Shaft} = [\bar{T}_\omega\ \ T_e\ \ 0]^T \quad (8)$$

$$A_{\text{shaft}} = \begin{bmatrix} \frac{(-D_t - D_{tg})}{2H_t} & \frac{D_{tg}}{2H_t} & \frac{-1}{2H_t} \\ \frac{D_{tg}}{2H_g} & \frac{(-D_t - D_{tg})}{2H_g} & \frac{1}{2H_g} \\ K_{tg}\omega_b & -K_{tg}\omega_b & 0 \end{bmatrix} \quad (9)$$

$$B_{shaft} = \begin{bmatrix} \frac{1}{2H_t} & 0 & 0 \\ 0 & \frac{1}{2H_g} & 0 \\ 0 & 0 & 1 \end{bmatrix} \quad (10)$$

where $\bar{\omega}_m$ and $\bar{\omega}_r$ are turbin shaft speed and generator rotor speed respectively. T_w and T_{tg} are wind torque and internal torque of two mass systems, T_w is obtained from the MPPT curve. D_t, D_g and D_{tg} are damping coefficient of turbine, generator and turbine-generator set respectively. H_t and H_g are inertia constants of turbine and generator, respectively. K_{tg} is the inertia constants of turbine and generator.

3) MODELING OF BACK TO BACK CONVERTER

Two converters, GSC and RSC, are connected by a DC link from the back to back converter. The function of these converters is to make the induction machine works with the Maximum Power Point Tracking (MPPT) curve to generate maximum power output safely [51]. The MPPT technique helps to extract maximum power output from the generator in every wind condition by adjusting the torque reference to the converters [52]. The MPPT data of the system is given in the Appendix. The RSC is responsible for maintaining the desired electromagnetic torque based on MPPT data and reactive power adjustment as per the grid requirement. GSC is responsible for maintaining DC link voltage and generator stator voltage. Since the switching frequency of these converters is very large compared to the frequency of SSR phenomena [12], these converters' dynamics are not considered for this study. Instead, the controllers of these converters are modelled as a pair of two PI controllers. So each converter will add four states to the system model [11].

4) DC LINK MODEL

The dynamics of DC bus interconnecting RSC and GSC is modeled as follows [11], [12].

$$-CV_{DC}\frac{dV_{DC}}{dt} = P_r + P_g \quad (11)$$

$$P_r = 0.5\left(v_{qr}i_{qr} + v_{dr}i_{dr}\right) \quad (12)$$

$$P_g = 0.5\left(v_{qg}i_{qg} + v_{dg}i_{dg}\right) \quad (13)$$

P_r and P_g are the active power injection at the rotor and grid side. V_{DC} is the voltage across the DC bus and C is the parallel capacitance across the DC bus.

5) TRANSMISSION LINE MODEL

The dynamics of the series compensated transmission line is modelled by considering line current and voltage across the

series capacitor as state variables [8], [53] and are given as,

$$\dot{X}_{Line} = A_{Line}X_{Line} + B_{Line}U_{Line} \tag{14}$$

$$X_{Line} = [i_{ql} \;\; i_{dl} \;\; v_{qc} \;\; v_{dc}]^T \tag{15}$$

$$U_{Line} = [-\frac{EB_q - v_{qs}}{X_L} \;\; -\frac{EB_d - v_{ds}}{X_L} \;\; 0 \;\; 0]^T \tag{16}$$

$$A_{Line} = \begin{bmatrix} -\frac{R_L}{X_L} & -1 & -\frac{1}{X_L} & 0 \\ 1 & -\frac{R_L}{X_L} & 0 & -\frac{1}{X_L} \\ X_C & 0 & 0 & -1 \\ 0 & X_C & 1 & 0 \end{bmatrix} \tag{17}$$

$$B_{Line} = \begin{bmatrix} \omega_b & 0 & 0 & 0 \\ 0 & \omega_b & 0 & 0 \\ 0 & 0 & 1 & 0 \\ 0 & 0 & 0 & 1 \end{bmatrix} \tag{18}$$

i_{ql}, i_{dl}, v_{qc} and v_{dc} are the d and q axis components of line current and voltage across the series capacitor respectively and EB_q and EB_d are the q and d axis components of infinite bus voltage. R_L, X_L and X_C are the transmission line resistance, line inductive reactance and series capacitive reactance.

Hence the entire system is represented by twenty states. The induction machine, RSC controller, GSC controller, and transmission line have four states each, the shaft system and DC link have three and one states, respectively. SSR possibilities in the system are studied using these 20 states; the abstract of these different states corresponding to each component is enlisted in Table 1.

TABLE 1. Various components and corresponding states of study system.

Components	States	Components	States
DFIG	i_{qs},i_{ds},i_{qr}, i_{dr},i_{0s},i_{0r}	DC Link	V_{DC}
RSC Controller	i^*_{qr},i^*_{dr}, v_{qr},v_{dr}	Shaft System	ω_m, ω_r,T_{tg}
GSC Controller	i^*_{qg},i^*_{dg}, v_{qg},v_{dg}	Series Compensated Line	i_{ql},i_{dl},v_{qc}, v_{dc},i_{0l},v_{0c}

C. OBSERVATIONS FROM EVA

The system's Eigenvalues are evaluated by linearising the nonlinear dynamic equations formulated in the previous section around an equilibrium point. The real part of the eigenvalue will indicate a particular mode's stability, whereas the imaginary part gives the oscillation frequency of that particular mode. For the system to be stable, all the modes should have a negative real part [54]. Since the study system is modelled using 20 states, the EVA will have 20 eigenvalues. The eigenvalues obtained for a wind speed of $7m/s$ with 50 % series compensation is given in Table 2. Parameters of the DFIG system are mentioned in the Appendix.

Among the 20 eigenvalues, only six pairs are oscillatory. They are

1) Higher frequency resonance mode ($\lambda_{1,2}$)
2) Super synchronous resonance mode ($\lambda_{3,4}$)
3) Subsynchronous resonance mode ($\lambda_{5,6}$)
4) Electro mechanical mode ($\lambda_{7,8}$)
5) Shaft mode ($\lambda_{9,10}$)
6) System mode ($\lambda_{11,12}$)

From Table 2, it is clear that except subsynchronous resonance mode, all other system modes have a negative real part. This indicates that the system is unstable due to subsynchronous resonance mode at 50 % series compensation and a wind speed of 7 m/s. For an oscillatory mode to have an impact on SSR instability, the frequency of the particular mode should be close to the subsynchronous complement of system frequency (50Hz or 314rad/sec). From Table 2, it is clear that the frequency of higher frequency resonance mode is 1088.10 rad/sec or 173.28 Hz, which is much higher than the system frequency. Hence the behaviour of higher frequency resonance mode is excluded from further analysis. Since the system mode is equally participating in all the states and the frequency of this mode is very close to complement of system frequency, the behaviour of this mode is not considered for SSR analysis [3], [20]. The methods to distinguish these modes and the detailed explanation for these modes' behaviour at various operating conditions were presented in the author's previous paper [55]. The behaviour of the remaining modes with the change in series compensation and change in wind speed is explained briefly here.

TABLE 2. Eigenvalue analysis of the study system at 50% compensation level and Wind Velocity of 7 *m/s*.

Mode	Eigen Value	Mode	Eigen Value
$\lambda_{1,2}$	$-2195.90 \pm 1088.10i$	λ_{14}	-0.33
$\lambda_{3,4}$	$-10.35 \pm 526.81i$	λ_{15}	-0.01
$\lambda_{5,6}$	$4.66 \pm 100.10i$	λ_{16}	-19.12
$\lambda_{7,8}$	$-13.06 \pm 79.79i$	λ_{17}	-10.03
$\lambda_{9,10}$	$-0.98 \pm 5.48i$	λ_{18}	-0.02
$\lambda_{11,12}$	$-0.06 \pm 0.49i$	λ_{19}	-1.68
λ_{13}	-25.65	λ_{20}	-0.11

1) BEHAVIOR OF SUPERSYNCHRONOUS MODE

Supersynchronous mode will be unstable only when the net resistance corresponding to supersynchronous frequency

$$A_{DFIG} = \begin{bmatrix} \frac{-\omega_b X_{rr} R_s}{X_{rr}X_{ss}-X_m^2} & \frac{(\omega_b-\omega_r)X_m^2-\omega_b X_{rr}X_{ss}}{X_{rr}X_{ss}-X_m^2} & \frac{\omega_b X_m R_r}{X_{rr}X_{ss}-X_m^2} & \frac{-\omega_r X_m X_{rr}}{X_{rr}X_{ss}-X_m^2} \\ \frac{\omega_b X_{rr}X_{ss}-(\omega_b-\omega_r)X_m^2}{X_{rr}X_{ss}-X_m^2} & \frac{-\omega_b X_{rr} R_s}{X_{rr}X_{ss}-X_m^2} & \frac{\omega_r X_m X_{rr}}{X_{rr}X_{ss}-X_m^2} & \frac{\omega_b X_m R_r}{X_{rr}X_{ss}-X_m^2} \\ \frac{\omega_b X_m R_s}{X_{rr}X_{ss}-X_m^2} & \frac{\omega_r X_m X_{ss}}{X_{rr}X_{ss}-X_m^2} & \frac{-\omega_b X_{ss} R_r}{X_{rr}X_{ss}-X_m^2} & \frac{\omega_b X_m^2-(\omega_b-\omega_r)X_{rr}X_{ss}}{X_{rr}X_{ss}-X_m^2} \\ \frac{-\omega_r X_m X_{ss}}{X_{rr}X_{ss}-X_m^2} & \frac{\omega_b X_m R_s}{X_{rr}X_{ss}-X_m^2} & \frac{(\omega_b-\omega_r)X_{rr}X_{ss}-\omega_b X_m^2}{X_{rr}X_{ss}-X_m^2} & \frac{-\omega_b X_{ss} R_r}{X_{rr}X_{ss}-X_m^2} \end{bmatrix} \tag{4}$$

seen from the generator side is negative. The analysis from the author's previous paper [55] shows that the resistance corresponding to supersynchronous frequency seen from the generator side will be positive for all possible wind speed and series compensation. Hence it can be concluded that for all operating cases, this mode will be stable.

2) BEHAVIOR OF SUBSYNCHRONOUS MODE

Whenever the net resistance corresponding to subsynchronous frequency seen from the generator side becomes negative, that leads to instability of the subsynchronous mode. The analysis found that lower wind speed and a higher level of series compensation can cause undamping of this mode. The phenomenon in which the system loses its stability when net resistance corresponding to the subsynchronous frequency seen from the generator becomes negative is termed as Induction Generator Effect (IGE) [55].

3) BEHAVIOR OF ELECTROMECHANICAL MODE

Electromechanical mode frequency is equivalent to the subsynchronous complement frequency of the turbine shaft system's mechanical natural frequency. As this mode is more connected with the study system's mechanical parameters, its stability depends more on wind speed. The change in series compensation has not much effect on this mode. The analysis found that this mode is stable for all wind speed and series compensation.

4) BEHAVIOR OF SHAFT MODE

This mode is more dependent on the stiffness of the generator shaft system. As long as the system's mechanical parameters are fixed, the frequency of this mode is also fixed. Since wind turbines have comparatively less stiffness than conventional generators, the shaft mode frequency will be small. For this mode to be unstable, the electrical, natural frequency of the system should have a frequency close to complement of the frequency of shaft mode. This can happen only at a higher level of series compensation. (Usually, the level of series compensation is restricted to 70-75 % due to load balancing with parallel path, high fault current, and load flow control issues [4]. So those percentage of compensation more than this is considered as a higher level of series compensation). Since transmission lines are not operating at such a higher level of series compensation, it is seen that the shaft mode is stable for all practical working conditions.

5) SUMMARY OF EVA

- At a higher level of series compensation, subsynchronous mode gets excited and leads to instability of the system.
- Higher wind speed drives the system to operate in stable operating conditions even with a higher level of series compensation.
- The only mode that gets unstable while increasing the series compensation level is the subsynchronous mode.
- SSR damping controller should be configured to damp the subsynchronous resonance mode for a higher level of series compensation.

The effect of wind speed, level of series compensation and stiffness of shaft system on SSCI was analyzed in [13], and similar observations were obtained. A higher level of series compensation and lower wind speed are causing SSCI oscillations in DFIG based wind farms. Moreover, the system with higher shaft stiffness is more venerable to SSCI oscillations [13].

The damping ratio and frequency of oscillation of modes changes with the change in system operating conditions. Nevertheless, the characteristics of the modes, such as states which are participating in a particular mode, will not change. The changes in operating conditions of the power system will eventually be reflected in the characteristics equation of the system transfer functions. Since the proposed method is developed based on the system's transfer function, the changes in operating points will eventually be accounted for in the method. In the author's previous work [55], it has been demonstrated that the instability of the system is mainly manifested in the subsynchronous mode for all possible operating conditions of wind speeds and levels of series compensation. Hence it is required to consider subsynchronous frequency mode for designing SDC to damp SSR DFIG based wind farms by ensuring that the proposed controller is not causing instability to other system modes.

III. BEST ICS-LOCATION PAIR SELECTION

The schematic diagram of the Sub-Synchronous Resonance Damping Controller (SSRDC) used in this work is shown in Fig 2. SSRDC consists of a simple proportional controller cascaded with a washout filter. The high pass washout filter is used to bypass the SSRDC action under steady-state operating conditions. The value of the time constant for the washout filter is considered as 5s [56]. Since the proposed work aims to formulate a procedure for finding out the best ICS-location pair, the SSRDC used in this work only validates the formulated procedure. Hence a simple proportional feedback controller based on the root locus method has been used. Since there are eight converter controllers, four in GSC controller and four in RSC controller, there are eight possible locations for placing SSRDC as shown in Fig 3 and Fig 4. In the case of ICS, any available variables can be considered for ICS. However, only eight variables are considered for the analysis. These are DC link voltage, the voltage across the series capacitor, generator stator voltage, power flowing

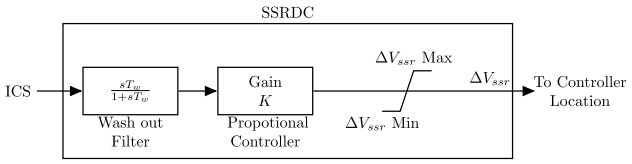

FIGURE 2. Schematic diagram of the SSRDC.

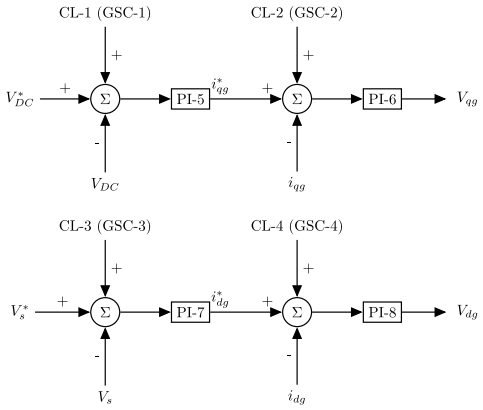

FIGURE 3. Possible locations for placing SSRDC in GSC controllers.

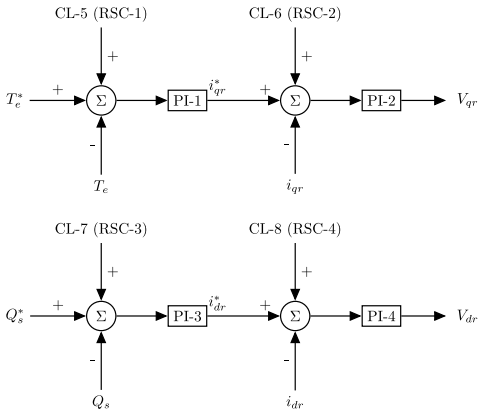

FIGURE 4. Possible locations for placing SSRDC in RSC controllers.

through the GSC and RSC converters, rotor speed, electromagnetic torque, and transmission line current. Since there are eight locations and eight ICS available, 64 ICS- location pairs are possible. Among these 64 pairs, the best pair has to be figured out. The systematic procedure for the selection is explained in the following section.

A. SELECTION PROCEDURE

The eigenvalue analysis shows that only subsynchronous mode appears to be unstable with the change in series compensation among the six oscillatory modes. So the damping controller is to be designed to damp the subsynchronous mode. The procedure to select the best available pair of ICS and location for the controller to damp the subsynchronous resonance can be described as follows.

Step 1: Identify the possible locations for placing SSRDC in DFIG; there are a total of eight locations available for placing SSRDC: four in GSC controller and four in RSC controller. These are shown in Fig 3 and Fig 4. The locations are named from $CL-1$ (control location-1) to $CL-8$. First, four locations, $CL-1$ to $CL-4$ are in the GSC controller, and the remaining four, $CL-5$ to $CL-8$ are in the RSC controller.

Step 2: Identify the available input control signals from the system. Readily available signals, as well as signals that can be estimated, are included in the list. In this analysis, eight signals are considered.

Step 3: Develop a state-space model of the system by considering voltage injection points at RSC and GSC controllers (location for placing SSRDC) as inputs and selected ICS as outputs. The state-space representation will be

$$\dot{X} = A * X + B * U \tag{19}$$

$$Y = C * X \tag{20}$$

where A is the state transition matrix, X represents the states of the system, Y denotes the output of the system (available ICS for SSRDC), U is the input to the system (voltage injecting points at RSC and GSC controller- locations for placing SSRDC), B and C are input and output matrices respectively.

Step 4: From the state space representation develop the transfer function matrix as

$$G = C * (SI - A)^{-1} \tag{21}$$

Each transfer function in the transfer function matrix, G, represents a pair of a particular SSRDC location and an ICS for SSRDC. For example, element G_{23} in the transfer function matrix G would correspond to the second ICS pair and third location ($CL-3/GSC-3$).

Step 5: For each transfer function in the transfer function matrix, G, plot the Right Half Plane Zero (RHPZ) plots. If any open-loop zero is encountered on the right half side of the s-plane in the 5 to 45 Hz (31.4 -282.6 rad/s) frequency region, then that pair of ICS and location should be discarded from further investigation.

Step 6: Calculate the Relative Gain Array (RGA) number for the remaining pairs from step 5 for the 5 to 45 Hz (31.4 −282.6 rad/s) frequency range. RGA is also a screening tool used to exclude pairs that are not suitable for decentralised control. The candidates with larger RGA values are excluded from further analysis, and those candidates having smaller RGA values are considered for Henkel Singular Value (HSV) analysis.

Step 7: Finally, the HSV value for the remaining pairs obtained from RGA analysis are calculated. The pair with the largest HSV (Henkel Singular Value) should be selected as the best pair. The second-best pair and the consecutive best pairs will be available from HSV analysis. HSV gives the system's joint controllability and observability index, which can be used to identify the best ICS-location combination.

B. CRITERIA FOR SELECTION

A brief introduction to the methods used for selecting the best ICS – location pair is discussed in this section. In this work, three approaches are analysed to formulate the selection procedure. The performance of the procedure is then compared with the residue analysis based selection method. Hence this section provides a short introduction to the residue method also. Consider a Multi-Input Multi-Output (MIMO) system

with state-space representation as represented in Eqn (19) and (20). From this, the transfer function matrix for the system can be derived as

$$G(s) = \frac{Y(s)}{U(s)} = C * (SI - A)^{-1} \tag{22}$$

Here I is the Identity matrix. For each transfer function in the transfer function matrix, G represents the transfer function for the corresponding input and output. For example, element G_{23} in the transfer function matrix G will correspond to the transfer function of the second output (second element of Y matrix) and third input (the third element of U matrix).

1) RIGHT-HALF PLANE ZEROES (RHP-ZEROS)

Consider a system with open-loop transfer function as G_{OL} and the open-loop transfer function can be expressed as

$$G_{OL} = \frac{Z_{OL}}{P_{OL}} \tag{23}$$

where Z_{OL} and P_{OL} are the zeros and poles of the open loop transfer function. The closed loop transfer function of the system with feedback gain K will be

$$G_{CL} = \frac{G_{OL} * K}{1 + G_{OL} * K} \tag{24}$$

Substituting Eqn 23 in Eqn 24,

$$G_{CL} = \frac{K * Z_{OL}}{P_{OL} + K * Z_{OL}} = K * \frac{Z_{CL}}{P_{CL}} \tag{25}$$

Hence, it can be understood that the zeros of the closed-loop transfer function would be the same as the zeros of the open-loop transfer function. Nevertheless, the location of closed-loop poles will move from open-loop pole position to open-loop zero position as feedback gain increases. If the open-loop system has a zero at the right half side of the s-plane, then the closed-loop pole will cross the imaginary axis and move towards the open-loop zero while increasing gain K. This contributes to system instability. In order to avoid this, it is necessary to have no open-loop zeros at the right half-side of the s-plane at the frequency range of interest [30]. In the analysis, open-loop zeros of all possible ICS-location pairs are plotted, and those pairs having zeros on the right half side of the s-plane in the desired frequency range are discarded. This method is considered as a primary screening method for screening out the most unsuitable options.

2) RELATIVE GAIN ARRAY (RGA)

RGA can analyse the impact of decentralised control. RGA is the ratio of the gains of the system under two extreme cases [30], [43]. In order to calculate the RGA for a particular transfer function, the gain for the corresponding transfer function is calculated for the required frequency at two extreme cases. The first case is that all other loops are open, and all other input changes are zero. Then in the second case, all other loops are closed, and all output changes are zero. The first case to second case gain ratio gives the RGA value for the specific transfer function. The pair with the minimum RGA value is considered the best choice. The RGA method filters out those pairs of ICS-location pairs that are not so suited for decentralised control. In this study, a single feedback based SSR damping controller is designed for damping SSR and hence the ICS- location pairs that are best suited for decentralised control is preferable.

3) HANKEL SINGULAR VALUES (HSV)

HSV is an advanced method based on controllability and observability principle. Unlike PBH test, mutual controllability and observability can be found using HSV technique [39], [44], [30]. Controllability Gramian matrix (P) is given by,

$$P = \int_0^\infty e^{A*t} * B * B^T * e^{A^T*t} * dt \tag{26}$$

Observability Gramian matrix (Q) is given by,

$$Q = \int_0^\infty e^{A^T*t} * C * C^T * e^{A*t} * dt \tag{27}$$

and Hankel singular value (σ) is given by,

$$\sigma_i = \sqrt{\lambda_i * P * Q} \tag{28}$$

Here λ_i is the eigenvalue corresponding to the i^{th} mode, A is the state transition matrix, B and C are input and output matrices, respectively. HSV for each input (ICS)- output (location for this study) pair should be calculated, and the pair with a maximum value of HSV should be selected as the best input (ICS)- output (location for this study) pair.

4) RESIDUE METHOD

The transfer function of a system can be represented as

$$G(s) = \frac{Y(s)}{U(s)} = \sum_{i=1}^{n} \frac{R_i}{S - \lambda_i} \tag{29}$$

$$G(s) = \frac{K * (S - Z_1) * (S - Z_2) * \ldots (S - Z_m)}{(S - P_1) * (S - P_2) * \ldots (S - P_n)} \tag{30}$$

$$R_i = C_k * V_i * W_i * B_j \tag{31}$$

where m is the number of zeros and n is the number of poles of the system. The number of poles equals the number of modes of the system. V_i and W_i are the right and left eigenvectors corresponding to the mode λ_i. C_k and B_j are the corresponding columns and row for k^{th} and j^{th} output and input. In residue analysis, the dynamics due to only one eigenvalue are considered by neglecting the dynamics of all other eigenvalues. Now the system gets reduced into a single-pole system with transfer function [3], [29], [30].

$$G(s) = \frac{R_i}{S - \lambda_i} \tag{32}$$

R_i is the residue value corresponding to the i^{th} mode, and the input-output pairs with larger residue values are considered as the optimal pair. Residues depend on the scale of the input and output signals and do not necessarily offer a reliable comparison among transfer functions associated with variables with different units. So the results of residue analysis cannot be interpreted explicitly. Hence, in this work, this method is used for comparison purposes only.

5) JOINT GEOMETRIC CONTROLLABILITY AND OBSERVABILITY MEASURE (JGCOM)

This method is based on the controllability and observability principles of linear systems. The geometric controllability ($G_{cg}(m)$) and observability ($G_{oh}(m)$) are defined as [40], [41]

$$G_{cg}(m) = \cos(B_g, \psi_m) = \frac{|B_g^T, \psi_m|}{\|\psi_m\| \|B_g^T\|} \tag{33}$$

$$G_{oh}(m) = \cos(C_h, \phi_m) = \frac{|C_h, \phi_m|}{\|\phi_m\| \|C_h\|} \tag{34}$$

where B_g and C_h are the g^{th} and h^{th} column and row of B and C matrix respectively. ψ_m and ϕ_m are the left and right eigenvectors of A matrix corresponding to m^{th} oscillation mode. || and ||| are the modulus and Euclidean norm of the matrix, respectively. The geometric measures provide how aligned the columns of matrix B and the rows of C are with an eigenvector of A. If $G_{cg}(m) = 0$, the column of B_g is orthogonal to eigenvector ψ_m and a controller will not be effective to modify the state associated with eigenvalue λ_k. Similarly, if $G_{oh}(m) = 0$; C_h and ϕ_m are orthogonal and mode λ_k will not be observable from the output. [34]. Since the geometric controlability and observability are unrelated to each other, to get the best controllable-observable pair, joint geometric controllability and observability measures are used. Which is the product of the above two, $G_{co}(gh) = G_{cg}(m) * G_{oh}(m)$. Geometric measures, like residues, provide similar information but have the advantage of being normalised and independent of signal scale.The combination with the highest value of the joint geometric controllability and observability measure is the best match.

IV. SELECTION OF BEST ICS-LOCATION PAIR

Total eight locations, four on the GSC controller and four on the RSC controller, are considered for the selection process. Electromagnetic torque, rotor speed, the current through the transmission line, active power flowing through GSC and RSC converters, voltages across the capacitor, DC link and DFIG stator winding are considered as ICS. Therefore, a total of eight locations and eight ICS requires 64 pairs to be checked.

A. RHPZ PLOTS

The right half-plane zero plots for all the 64 pairs have been mapped, and the result obtained from the RHPZ analysis are tabulated in Table 3. From Table 3, the pairs with open-loop zeros on the right side of the s-plane in the 5 to 45 Hz (31.4 -282.6 rad/s) frequency range were observed and ruled out from further evaluation. From the RHPZ plots, it is evident that only ten pairs among the 64 are suitable for further analysis. It is worth noting that control locations $GSC3$, $GSC4$, $RSC1$ and $RSC2$ have open-loop zeros in the right half side of the s-plane in the desired frequency range. So these locations are completely excluded from further analysis. A similar observation can be made for ICS such as I_L, W_r, T_e and P_r. Hence these inputs are also completely excluded from further analysis.

TABLE 3. ICS-location pair having open loop zeros on right half of s-plane.

	GSC1	GSC2	GSC3	GSC4	RSC1	RSC2	RSC3	RSC4
V_C	No	No	Yes	Yes	Yes	Yes	Yes	Yes
I_L	Yes	Yes	Yes	Yes	Yes	Yes	Yes	Yes
W_r	Yes	Yes	Yes	Yes	Yes	Yes	Yes	Yes
V_S	No	No	Yes	Yes	Yes	Yes	No	No
T_e	Yes	Yes	Yes	Yes	Yes	Yes	Yes	Yes
V_{DC}	No	No	Yes	Yes	Yes	Yes	Yes	Yes
P_g	No	No	Yes	Yes	Yes	Yes	Yes	Yes
P_r	Yes	Yes	Yes	Yes	Yes	Yes	Yes	Yes

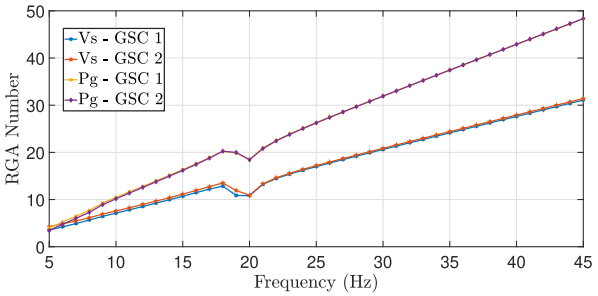

FIGURE 5. ICS-location pairs with large RGA values.

B. RGA

The relative gain array number for all the ten pairs obtained from the RHPZ method are calculated for the 5 to 45 Hz (31.4 -282.6 rad/s) frequency range. The analysis shows that four pairs have a significantly higher value of the RGA number. They are $V_S - GSC1$, $V_S - GSC2$, $P_g - GSC1$, and $P_g - GSC2$. The RGA plot for these pairs is given in Fig. 5. On the other hand, RGA numbers of the other six pairs have lower values, which are considered for further analysis. They are $V_{DC} - GSC2$, $V_C - GSC2$, $V_S - RSC3$, $V_{DC} - GSC1$, $V_C - GSC1$, and $V_S - RSC4$. The RGA plot for those pairs is given in Fig 6.

C. HSV

The Hankel singular values corresponding to those six pairs obtained from RGA analysis are calculated for the desired frequency range and plotted in Fig 7 and 8. The pairs with large Hankel singular values are considered as the best choices. The best ICS-location selection list obtained from the HSV method is given in Table 4. Table 4 show that the best possible pair is $V_{DC} - GSC2$, the second preferred choice is $V_C - GSC2$, and the least preferred pair is $V_S - RSC3$. From HSV, it is found that the second-best choice is pair $V_C - GSC2$ and pair $V_{DC} - GSC1$ is the fourth-best choice.

V. VALIDATION OF THE PROPOSED STRATEGY

Validation of the proposed algorithm is achieved by implementing SSRDC at the identified locations with the

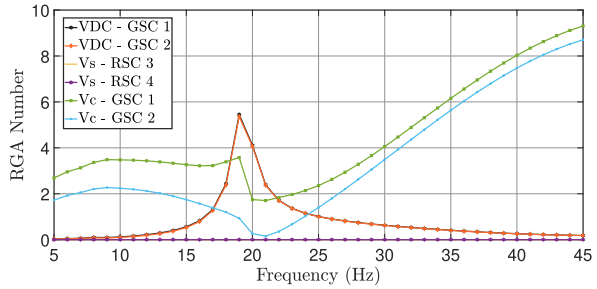

FIGURE 6. ICS-location pairs with lower RGA values.

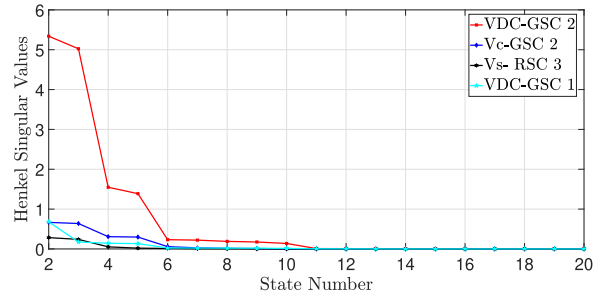

FIGURE 7. ICS-location pairs with large HSV values.

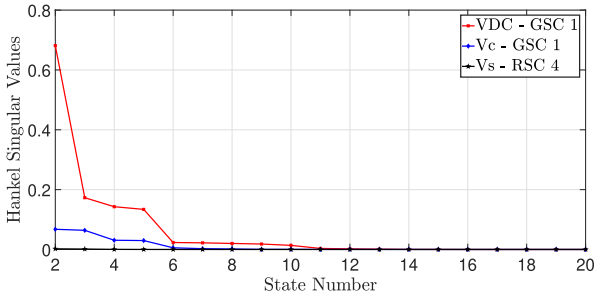

FIGURE 8. ICS-location pairs with lower HSV values.

corresponding input signal as the ICS for the controller. A supplementary damping controller to the existing DFIG converter controllers, which is a proportional feedback controller appended, is designed by the root locus method and is considered for the study. Since the intention is to validate the proposed strategy, a classic proportional feedback controller is used as SSRDC. The gain value for the proportional controller is found out by using the root locus method. The root locus diagram for the transfer function corresponding to the selected ICS-location pair ($V_{DC}-GSC2$) is plotted and given in Fig 9. From the figure, the gain corresponding to the subsynchronous mode for a damping ratio of 5 percentage is obtained as 4.2. Fig 9 depicts shifting of closed loop poles from the right half side of the s-plane to the stable left half side while the value of gain, K, increase from zero to infinity. At $K = 4.2$, the subsynchronous mode attains a five percentage damping level, and this value of gain is selected for designing a proportional controller. Here the selection of the damping ratio is arbitrary. The behaviour of subsynchronous

TABLE 4. The best ICS-location selection list obtained from HSV method.

First Choice	$V_{DC} - GSC2$	Fourth Choice	$V_{DC} - GSC1$
Second Choice	$V_C - GSC2$	Fifth Choice	$V_C - GSC1$
Third Choice	$V_S - RSC4$	Sixth Choice	$V_S - RSC3$

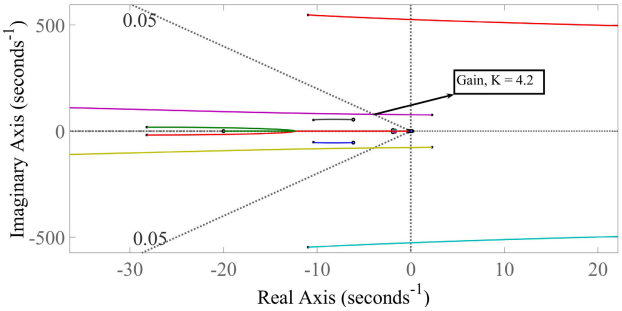

FIGURE 9. Root locus diagram for the transfer function corresponding to $V_{DC} - GSC\ 2$ pair.

mode and other oscillatory modes while placing SSRDC with various ICS-location pairs is demonstrated in Table 5. The corresponding value of gain, K for the five percentage damping ratio obtained by root locus method, is also provided in Table 5. The table shows that the value of gain, K, is increasing when moving down the ICS-location priority list, which justifies the proposed method.

A. TIME DOMAIN SIMULATION RESULTS

In order to validate the proposed strategy, the time-domain simulation of the system is performed using MATLAB/Simulink. The performance of the SSRDC with the first three ICS – location combinations obtained by the proposed procedure is analysed for a wind speed of 8m/s. Initially, the series compensation is kept as 40%, but at time $t = 5s$ series compensation is changed to 70%. This switching action triggers a disturbance in the system. This disturbance excites SSR mode and leads to undamped oscillations if SSRDC is not provided. By the introduction of SSRDC based on the proposed method with proper choice of location and input signals, SSR oscillations are damped out, and the results are shown in Fig 10. It shows the response of active power for the three cases. The plot shows that the SSR damping by SSRDC based on the first choice with the proposed procedure is better than that of the consecutive choices. Choice 1 imparts better damping than choice 2, and similarly, choice 2 is better than choice 3. This substantiates the observations from the analytical study of the proposed procedure.

B. COMPARISON OF PROPOSED METHOD WITH OTHER METHODS

The results obtained by the proposed method is compared with the results obtained by the residue-based method and joint geometric controllability method. For comparison purposes, the most unsuitable combinations with open-loop zero on the right half side of the s-plane have been filtered out using the RHPZ method. Hence the total number is reduced

TABLE 5. The behavior of different oscillatory modes while placing SSRDC based on various ICS- location pairs at 60 % series compensation and Wind Velocity of 7 *m/s*.

MODES	Without SSRDC	$V_{DC}-GSC2$	V_C-GSC2	V_S-RSC4	$V_{DC}-GSC1$	V_C-GSC1	V_S-RSC3
Gain, K		4.2	8.3	21.7	46	52.3	71.3
Higher Frequency Mode	-2187.4 $\pm 1078.1i$	-329.27 $\pm 1069.7i$	-2450.1 $\pm 1016.5i$	-1354 $\pm 1064.74i$	-329.27 $\pm 1069.7i$	-2038.7 $\pm 1176.3i$	-1758.1 $\pm 2417.3i$
Super synchronous Mode	-11.22 $\pm 547.06i$	-10.05 $\pm 546.55i$	-6.02 $\pm 536.57i$	-11.20 $\pm 547.04i$	-10.07 $\pm 548.78i$	-1.52 $\pm 556.26i$	-2.04 $\pm 528.92i$
Subsynchronous Mode	8.67 $\pm 89.301i$	-4.88 $\pm 90.54i$	-4.86 $\pm 92.62i$	-4.73 $\pm 90.74i$	-4.32 $\pm 85.69i$	-4.26 $\pm 88.29i$	-4.37 $\pm 89.56i$
Electro Mechanical Mode	-16.83 $\pm 70.34i$	-17.96 $\pm 76.68i$	-22.29 $\pm 74.38i$	-13.93 $\pm 75.98i$	-08.41 $\pm 68.46i$	-05.53 $\pm 71.83i$	-14.30 $\pm 67.98i$
Shaft Mode	-27.28 $\pm 18.69i$	-21.05 $\pm 19.65i$	-21.98 $\pm 17.24i$	-8.138 $\pm 17.07i$	-10.27 $\pm 18.78i$	-24.30 $\pm 17.98i$	-08.34 $\pm 20.13i$
System Mode	-1.06 $\pm 5.42i$	-1.13 $\pm 5.68i$	-1.06 $\pm 5.49i$	-1.02 $\pm 5.48i$	-1.18 $\pm 5.68i$	-0.95 $\pm 5.28i$	-1.71 $\pm 5.22i$

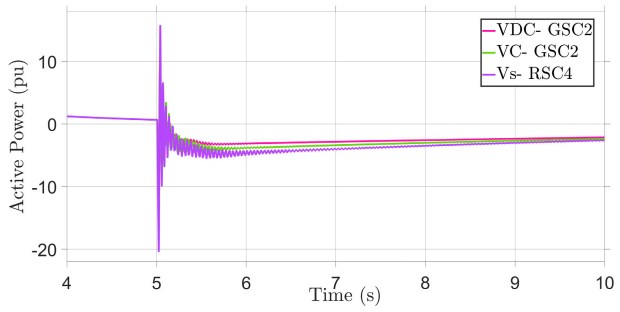

FIGURE 10. Dynamic response of active power with SSRDC implemented at the first three ICS – location combinations obtained by the proposed procedure by changing the level of series compensation from 40 % to 70 % at $t = 5s$ for a wind speed of 8 *m/s*.

to ten from 64. The observation from the comparison is explained below.

1) COMPARISON OF PROPOSED METHOD WITH RESIDUE ANALYSIS

The residue values corresponding to the subsynchronous mode for the ten pairs obtained by conducting RHPZ analysis are listed in Table 6. The results obtained from the proposed method are compared with the result of residue analysis and given in Table 8. Proposed method and residue analysis yield the same results for the first two choices. However, the third and fifth choices are different. The fourth preference is found to be the same with both methods. This variation arises because the residue relies on the scale of input and output signals. The third preferred choice from the residue method is not indicated by the proposed method. Under such circumstances, the residue analysis cannot be considered reliable. The comparison of residue values is meaningful only if all the ICS are of the same type. In this case, a different set of signals such as machine voltages, currents, speed, and power are involved [39]. In addition to that, residue analysis considers only one mode at a time and the performance of SDC affects the stability of other modes [33]. Hence, a detailed procedure proposed in this paper can be employed for selecting the most suitable ICS and the best location for placing SSRDC.

TABLE 6. Preferable input-location pairs by residue method.

Sl. No	Input – location pair	Residue corresponding to subsynchronous mode
1	$V_{DC}-GSC2$	12.967
2	V_C-GSC2	5.315
3	V_S-GSC2	1.450
4	$V_{DC}-GSC1$	1.307
5	P_g-GSC2	0.631
6	V_C-GSC1	0.536
7	V_S-GSC4	0.146
8	P_g-GSC1	0.064
9	V_S-RSC8	0.011
10	V_S-RSC7	0.001

TABLE 7. Joint geometric controllability and observability values correspond to subsynchronous resonance mode for all possible ICS and SDC locations combinations.

	GSC1	GSC2	GSC3	GSC4	RSC1	RSC2	RSC3	RSC4
V_C	0.080	0.080	0.093	0.093	1e-5	1e-8	0.002	0.311
I_L	0.139	0.139	0.162	0.162	1e-5	1e-8	0.003	0.543
W_r	1e-5	1e-5	1e-5	1e-5	1e-5	1e-8	1e-6	0.001
V_S	0.013	0.013	0.015	0.015	1e-5	1e-8	0.001	0.049
T_e	0.029	0.029	0.034	0.034	1e-5	1e-8	0.001	0.115
V_{DC}	0.110	0.110	0.127	0.127	1e-5	1e-8	0.003	0.427
P_g	0.018	0.018	0.021	0.021	1e-5	1e-8	0.001	0.069
P_r	0.039	0.039	0.045	0.045	1e-5	1e-8	0.001	0.149

TABLE 8. Comparison of proposed method with residue method and JGCO method.

Input – location pair	Preference obtained by proposed method	Preference obtained by residue method	Preference obtained by JGCO method
$V_{DC}-GSC2$	1	1	1
V_C-GSC2	2	2	3
V_S-RSC4	3	9	9
$V_{DC}-GSC1$	4	4	2
V_C-GSC1	5	6	6
V_S-RSC3	6	10	4

TABLE 9. Comparison of proposed method with RGA and HSV analysis conducted independently.

Preference order	Preference obtained by proposed method	Preference obtained by RGA method alone	Preference obtained by HSV method alone
1	$V_{DC}-GSC2$	P_r-GSC2	ω_r-GSC4
2	V_C-GSC2	P_r-GSC1	ω_r-GSC3
3	V_S-RSC4	P_r-GSC3	$V_{DC}-GSC4$
4	$V_{DC}-GSC1$	P_r-GSC4	$V_{DC}-GSC2$
5	V_C-GSC1	V_S-RSC3	i_l-GSC4
6	V_S-RSC3	V_S-RSC4	P_g-GSC4

2) COMPARISON OF PROPOSED METHOD WITH JOINT GEOMETRIC CONTROLLABILITY AND OBSERVABILITY METHOD (JGCOM)

The joint geometric controllability and observability values corresponding to subsynchronous resonance mode for all the possible combinations of the input control signal and SDC locations are evaluated and is given in Table 7. The combinations having larger values are to be considered as preferred choices. The comparison of the result obtained from the proposed procedure and the joint geometric method and is given in Table 8. From the Table 8, it is evident that the first choice is the same from all the methods. However, the results are not identical for the remaining choices. This is because in addition to the joint controllability and observability property, the choice most suited for decentralised control application is selected using RGA method in the proposed method. However, this kind of filtering is not possible by the JGCOM. By the JGCOM method, the combinations having maximum controllable and observable properties can be find out. But that does not confirm that they are suitable for decentralised control applications.

Mitigation of SSCI oscillations on DFIG based wind farms was achieved by proper tuning of the RSC and GSC controller parameters in [13]. Like that work, in this paper also DFIG converter controllers have been used for SSR damping in DFIG based wind farms. Unlike that work, the ICS and location for SSRDC are selected based on a systematic procedure. The impact of controller parameters on SSCI was explained in [13]. Since the scope of this work is limited to the study of SSR analysis only, the study of damping controller parameters changes on SSCI oscillations is suggested as future work.

C. JUSTIFICATION OF PROPOSED METHOD

The proposed method is validated by comparing the observations from the proposed procedure with the observations based on independently conducting RGA analysis and HSV analysis. The list of best ICS-location choices obtained by conducting RGA analysis and HSV analysis independently is given in Table 9 along with the choice preferences of the proposed procedure. From Table 9, it can be concluded that the first four choices made by conducting RGA analysis independently cannot be considered for designing SSRDC. Since from RHPZ plots, it is identified that all choices involving ICS P_r are not suitable due to the open-loop zero at the right side of the s-plane. This shows that the observations based on RGA analysis alone would not be reliable. Similarly, the first two and last two choices obtained by conducting HSV analysis alone are also not acceptable. Because, from RHPZ plots, it is identified that all choices involving $GSC3$ and $GSC4$ are unacceptable due to the presence of open-loop zero on the right half side of the s-plane. Hence from these two observations, it can be concluded that the selection of ICS-location pair made by conducting RGA and HSV analysis independently would not result in the best choices. So, the best ICS – location pair should be selected by conducting RHPZ analysis, RGA analysis and HSV analysis simultaneously as per the proposed procedure detailed in this work.

Here RHPZ method is used as a primary screening method to filter out the ICS- location combinations having open-loop zeros on the right half side of the s-plane that are not suited for control application. The computational complexity can be reduced substantially by eliminating the vast number of unsuitable choices from further analysis by the RHPZ method. A decentralised control strategy is required since the proposed SDC has to control the MIMO system using a single controller. So the ICS-location pair selected should be suitable for decentralised control applications. Hence the combinations of ICS-location pairs that are not suited for decentralised control application is filtered out using the RGA method. Like the RHPZ method, the RGA method is also used as a screening method to filter out those choices which are not suited for decentralised control applications. Hence RGA method is executed in the second stage. In the last stage, the choices remaining from the previous stage are sorted based on joint controllability and observability index using the HSV method. Here HSV method is not used as an elimination method but only to sort the combinations in joint controllability index. If HSV analysis has been conducted before the RGA method, then more combinations have to be considered for HSV analysis. So for reducing the computational complexity without compromising on the outcome, the proposed procedure is sequenced in this pattern.

This paper addresses the selection of the best input-location pair for designing SSRDC to damp SSR in DFIG based wind farms based on a systematic procedure. The dynamics of PLL is not included in this analysis. The interaction between phase-locked loop (PLL) and weak grid can result in the instability of doubly-fed Induction generator (DFIG)-based wind power systems [57], [58]. This is because the weak grid introduces an open-loop zero in the right half side of the s-plane, and this will eventually result in oscillation at low power output as well as undamped oscillations at high power output [59]. Since the proposed procedure filters out the input-location combinations having open loop zero at the right half side of the s-plane using the RHPZ method, the effect of PLL dynamics does not alter the selected input-location pair through the proposed method. However, for designing an optimum damping controller,

detailed multi-machine modelling with PLL dynamics is required [26] and is beyond the scope of this paper. The proportional feedback controller designed in section V is used to validate the proposed procedure. Hence the design of SSRDC for mitigating SSR in DFIG based wind farms by incorporating PLL dynamics and multi-machine modelling of the study system is proposed as future work.

VI. CONCLUSION

The performance of the SDC for damping SSR oscillations in DFIG based wind farms highly depends on its ICS-location pair selected. Hence, this paper proposes a strategy for selecting the best location and best input control signal for the supplementary damping controller based on RHPZ plots, RGA method and HSV analysis. The best input control signal obtained by the proposed procedure for designing SSRDC is the voltage across the DC link, and the best location for providing SSRDC is identified as *GSC*2. In order to validate the proposed procedure, a proportional feedback controller is designed based on the root locus method, and the behaviour of all oscillatory modes with SSRDC placed is observed. A time-domain simulation analysis using MATLAB/Simulink is conducted by introducing SSRDC to the existing DFIG converter controllers based on the proposed procedure's first three choices. On analysis, the first choice made by the proposed procedure has better damping compared to the consecutive choices. This validates the proposed procedure. Observations based on the proposed method is then compared with the results of the residue-based analysis and joint geometric controllability method. The justification of the proposed procedure is made by comparing the results obtained from the proposed method with RGA analysis and HSV analysis done independently. The proposed procedure is applicable for DFIG based wind farms to select the best ICS-location choice for designing SDC to damp SSR when multiple signals and locations are available for selection. The design of a sliding mode controller based SSRDC for mitigating SSR in DFIG based wind farms constituting the multi-machine system, including the Phase-Locked Loop (PLL) dynamics is considered for future research.

APPENDICES

See Table 10, 11 and 12.

TABLE 10. Parameters of the single 2 MW and 100 MW aggregated DFIG. (Values given are in pu).

Base power	2 MW	100 MW
Base voltage (V_{LL})	690 V	690 V
X_{ls}	0.09231	0.09231
X_{lr}	0.09955	0.09955
X_M	3.95279	3.95279
R_s	0.00488	0.00488
R_r	0.00549	0.00549
X_{tg}	0.3	0.3 pu
DC Link base voltage	1200 V	1200 V
DC Link capacitor	14000 μF	50*14000 μF

TABLE 11. Parameters of the network and the shaft system.

Transformer ratio	690/161 kV	H_t	4.29 pu
Base MVA	100 MVA	H_g	0.90 pu
R_{line}	0.02 pu	D_t	0.00 pu
X_{line}	0.50 pu	D_g	0.00 pu
X_T	0.14 pu	D_{tg}	1.50 pu
X_s	0.06 pu	K_{tg}	0.15 pu

TABLE 12. MPPT Curve Data of the DFIG sytsem.

Wind velocity $v(m/s)$	7	8	9	10	11	12
ω_r (pu)	0.75	0.85	0.95	1.05	1.15	1.25
Power (pu)	0.32	0.49	0.69	0.95	1.25	1.6
Torque (pu)	0.42	0.57	0.72	0.90	1.08	1.28

REFERENCES

[1] G. Abad, J. Lopez, M. Rodriguez, L. Marroyo, and G. Iwanski, *Doubly Fed Induction Machine: Modeling and Control for Wind Energy Generation*, vol. 85. Hoboken, NJ, USA: Wiley, 2011.
[2] M. A. Chowdhury and G. M. Shafiullah, "SSR mitigation of series-compensated DFIG wind farms by a nonlinear damping controller using partial feedback linearization," *IEEE Trans. Power Syst.*, vol. 33, no. 3, pp. 2528–2538, May 2018.
[3] L. Fan and Z. Miao, "Mitigating SSR using DFIG-based wind generation," *IEEE Trans. Sustain. Energy*, vol. 3, no. 3, pp. 349–358, Jul. 2012.
[4] N. G. Hingorani and L. Gyugyi, *Understanding FACTS*. New York, NY, USA: IEEE Press, 2000.
[5] Y. Xia, B. K. Johnson, Y. Jiang, N. Fischer, and H. Xia, "A new method based on artificial neural network, wavelet transform and short time Fourier transform for subsynchronous resonance detection," *Int. J. Elect. Power Energy Syst.*, vol. 103, pp. 377–383, Dec. 2018.
[6] M. Abdeen, H. Li, and L. Jing, "Improved subsynchronous oscillation detection method in a DFIG-based wind farm interfaced with a series-compensated network," *Int. J. Electr. Power Energy Syst.*, vol. 119, Jul. 2020, Art. no. 105930.
[7] Q. Zhou, Y. Ding, K. Mai, X. Bian, and B. Zhou, "Mitigation of sub-synchronous oscillation in a VSC-HVDC connected offshore wind farm integrated to grid," *Int. J. Elect. Power Energy Syst.*, vol. 109, pp. 29–37, Jul. 2019.
[8] K. Padiyar, *Analysis of Subsynchronous Resonance in Power Systems*. Springer, 2012.
[9] W. Du, Y. Wang, and H. F. Wang, "Frequency drift of sub-synchronous oscillations caused by the DFIG wind farms when the wind speed varies," *Int. J. Electr. Power Energy Syst.*, vol. 103, pp. 317–325, Dec. 2018.
[10] R. Li, S. Zhao, B. Gao, R. Zhang, and Y. Hu, "Sub synchronous torsional interaction of steam turbine under wind power oscillation in wind-thermal power bundled transmission system," *Int. J. Electr. Power Energy Syst.*, vol. 108, pp. 445–455, Jun. 2019.
[11] L. Fan and Z. Miao, *Modeling and Analysis of Doubly Fed Induction Generator Wind Energy Systems*. New York, NY, USA: Academic, 2015.
[12] H. A. Mohammadpour and E. Santi, "Analysis of sub-synchronous resonance (SSR) in doubly-fed induction generator (DFIG)-based wind farms," *Synth. Lectures Power Electron.*, vol. 5, no. 3, pp. 1–64, Sep. 2015.
[13] B. Zoghdar-Moghadam-Shahrekohne and S. M. Barakati, "A novel approach for mitigating SSR in DFIG-based wind farms integrated into series compensated network," in *Proc. 9th Int. Congr. Ultra Modern Telecommun. Control Syst. Workshops (ICUMT)*, Nov. 2017, pp. 311–317.
[14] J. Shair, X. Xie, L. Wang, W. Liu, J. He, and H. Liu, "Overview of emerging subsynchronous oscillations in practical wind power systems," *Renew. Sustain. Energy Rev.*, vol. 99, pp. 159–168, Jan. 2019.
[15] M. S. El-Moursi, B. Bak-Jensen, and M. H. Abdel-Rahman, "Novel STATCOM controller for mitigating SSR and damping power system oscillations in a series compensated wind park," *IEEE Trans. Power Electron.*, vol. 25, no. 2, pp. 429–441, Feb. 2010.

[16] L. Wang and D.-N. Truong, "Stability enhancement of a power system with a PMSG-based and a DFIG-based offshore wind farm using a SVC with an adaptive-network-based fuzzy inference system," *IEEE Trans. Ind. Electron.*, vol. 60, no. 7, pp. 2799–2807, Jul. 2013.

[17] H. Jiang, R. Song, N. Du, P. Zhou, B. Zheng, Y. Han, and D. Yang, "Application of UPFC to mitigate SSR in series-compensated wind farms," *J. Eng.*, vol. 2019, no. 16, pp. 2505–2509, Mar. 2019.

[18] X. Zhu, M. Jin, X. Kong, J. Zhao, J. Liu, and Q. Zhou, "Subsynchronous resonance and its mitigation for power system with unified power flow controller," *J. Modern Power Syst. Clean Energy*, vol. 6, no. 1, pp. 181–189, Jan. 2018.

[19] A. Moharana, R. K. Varma, and R. Seethapathy, "SSR alleviation by STATCOM in induction-generator-based wind farm connected to series compensated line," *IEEE Trans. Sustain. Energy*, vol. 5, no. 3, pp. 947–957, 2014.

[20] H. A. Mohammadpour and E. Santi, "SSR damping controller design and optimal placement in rotor-side and grid-side converters of series-compensated DFIG-based wind farm," *IEEE Trans. Sustain. Energy*, vol. 6, no. 2, pp. 388–399, Apr. 2015.

[21] M. Mokhtari, J. Khazaei, and D. Nazarpour, "Sub-synchronous resonance damping via doubly fed induction generator," *Int. J. Electr. Power Energy Syst.*, vol. 53, pp. 876–883, Dec. 2013.

[22] Z. Bin, L. Hui, W. Mingyu, C. Yaojun, L. Shengquan, Y. Dong, Y. Chao, H. Yaogang, and C. Zhe, "An active power control strategy for a DFIG-based wind farm to depress the subsynchronous resonance of a power system," *Int. J. Electr. Power Energy Syst.*, vol. 69, pp. 327–334, Jul. 2015.

[23] Y. Wang, Q. Wu, R. Yang, G. Tao, and Z. Liu, "H_∞ current damping control of DFIG based wind farm for sub-synchronous control interaction mitigation," *Int. J. Electr. Power Energy Syst.*, vol. 98, pp. 509–519, Jun. 2018.

[24] P. Li, J. Wang, F. Wu, and H. Li, "Nonlinear controller based on state feedback linearization for series-compensated DFIG-based wind power plants to mitigate sub-synchronous control interaction," *Int. Trans. Electr. Energy Syst.*, vol. 29, no. 1, p. e2682, Jan. 2019.

[25] P. Li, L. Xiong, F. Wu, M. Ma, and J. Wang, "Sliding mode controller based on feedback linearization for damping of sub-synchronous control interaction in DFIG-based wind power plants," *Int. J. Elect. Power Energy Syst.*, vol. 107, pp. 239–250, May 2019.

[26] P. Li, J. Wang, L. Xiong, and M. Ma, "Robust nonlinear controller design for damping of sub-synchronous control interaction in DFIG-based wind farms," *IEEE Access*, vol. 7, pp. 16626–16637, 2019.

[27] P. Li, J. Wang, L. Xiong, S. Huang, M. Ma, and Z. Wang, "Energy-shaping controller for DFIG-based wind farm to mitigate subsynchronous control interaction," *IEEE Trans. Power Syst.*, vol. 36, no. 4, pp. 2975–2991, Jul. 2021.

[28] P. Li, L. Xiong, M. Ma, S. Huang, Z. Zhu, and Z. Wang, "Energy-shaping L_2-gain controller for PMSG wind turbine to mitigate subsynchronous interaction," *Int. J. Electr. Power Energy Syst.*, vol. 135, Feb. 2022, Art. no. 107571.

[29] N. N. Shah and S. R. Joshi, "Analysis, reduction and robust stabiliser design of sub-synchronous resonance in an IEEE FBM augmented by DFIG-based wind farm," *IET Renew. Power Gener.*, vol. 13, no. 16, pp. 3151–3167, Dec. 2019.

[30] S. Skogestad and I. Postlethwaite, *Multivariable Feedback Control: Analysis and Design*, vol. 2. New York, NY, USA: Wiley, 2007.

[31] K. Zhou, J. Doyle, and K. Glover, "Robust and optimal control," *Control Eng. Pract.*, vol. 4, no. 8, pp. 1189–1190, 1996.

[32] R. L. Williams and D. A. Lawrence, *Linear State-Space Control Systems*. Hoboken, NJ, USA: Wiley, 2007.

[33] M. M. Farsangi, Y. H. Song, and K. Y. Lee, "Choice of FACTS device control inputs for damping interarea oscillations," *IEEE Trans. Power Syst.*, vol. 19, no. 2, pp. 1135–1143, May 2004.

[34] J. L. Domínguez-García, C. E. Ugalde-Loo, F. Bianchi, and O. Gomis-Bellmunt, "Input–output signal selection for damping of power system oscillations using wind power plants," *Int. J. Electr. Power Energy Syst.*, vol. 58, pp. 75–84, Jun. 2014.

[35] H. Liu, X. Xie, Y. Li, H. Liu, and Y. Hu, "Mitigation of SSR by embedding subsynchronous notch filters into DFIG converter controllers," *IET Gener., Transmiss. Distrib.*, vol. 11, no. 11, pp. 2888–2896, Mar. 2017.

[36] S. O. Faried, I. Unal, D. Rai, and J. Mahseredjian, "Utilizing DFIG-based wind farms for damping subsynchronous resonance in nearby turbine-generators," *IEEE Trans. Power Syst.*, vol. 28, no. 1, pp. 452–459, Feb. 2013.

[37] U. Karaagac, S. O. Faried, J. Mahseredjian, and A.-A. Edris, "Coordinated control of wind energy conversion systems for mitigating subsynchronous interaction in DFIG-based wind farms," *IEEE Trans. Smart Grid*, vol. 5, no. 5, pp. 2440–2449, Sep. 2014.

[38] A. E. Leon and J. A. Solsona, "Sub-synchronous interaction damping control for DFIG wind turbines," *IEEE Trans. Power Syst.*, vol. 30, no. 1, pp. 419–428, Jan. 2015.

[39] B. Pal and B. Chaudhuri, *Robust Control in Power System*. Springer, 2006.

[40] T. Surinkaew and I. Ngamroo, "Inter-area oscillation damping control design considering impact of variable latencies," *IEEE Trans. Power Syst.*, vol. 34, no. 1, pp. 481–493, Jan. 2019.

[41] M. E. C. Bento, "Fixed low-order wide-area damping controller considering time delays and power system operation uncertainties," *IEEE Trans. Power Syst.*, vol. 35, no. 5, pp. 3918–3926, Sep. 2020.

[42] T. Prakash, V. P. Singh, and S. R. Mohanty, "A synchrophasor measurement based wide-area power system stabilizer design for inter-area oscillation damping considering variable time-delays," *Int. J. Electr. Power Energy Syst.*, vol. 105, pp. 131–141, Feb. 2019.

[43] Y. Li, C. Rehtanz, S. Ruberg, L. Luo, and Y. Cao, "Assessment and choice of input signals for multiple HVDC and FACTS wide-area damping controllers," *IEEE Trans. Power Syst.*, vol. 27, no. 4, pp. 1969–1977, Nov. 2012.

[44] M. M. Farsangi, Y. H. Song, and K. Y. Lee, "On selection of supplementary input signals for STATCOM to damp inter-area oscillations in power systems," in *Proc. IEEE Power Eng. Soc. Gen. Meeting*, vol. 3, Jun. 2005, pp. 3068–3073.

[45] P. M. Anderson, B. L. Agrawal, and J. E. Van Ness, *Subsynchronous Resonance in Power Systems*, vol. 9. Hoboken, NJ, USA: Wiley, 1999.

[46] H. A. Mohammadpour, A. Ghaderi, and E. Santi, "Analysis of subsynchronous resonance in doubly-fed induction generator-based wind farms interfaced with gate–controlled series capacitor," *IET Gener., Transmiss. Distrib.*, vol. 8, no. 12, pp. 1998–2011, Dec. 2014.

[47] T. E. Bechert and N. Chen, "First benchmark model for computer simulation of subsynchronous resonance," *IEEE Trans. Power App. Syst.*, vol. PAS-96, no. 5, pp. 1565–1572, Sep. 1977.

[48] Z. Miao, "Impedance-model-based SSR analysis for type 3 wind generator and series-compensated network," *IEEE Trans. Energy Convers.*, vol. 27, no. 4, pp. 984–991, Dec. 2012.

[49] L. M. Fernández, F. Jurado, and J. R. Saenz, "Aggregated dynamic model for wind farms with doubly fed induction generator wind turbines," *Renew. Energy*, vol. 33, pp. 129–140, Jan. 2008.

[50] L. M. Fernández, C. A. García, J. R. Saenz, and F. Jurado, "Equivalent models of wind farms by using aggregated wind turbines and equivalent winds," *Energy Convers. Manage.*, vol. 50, no. 3, pp. 691–704, Mar. 2009.

[51] C. Zhu, L. Fan, and M. Hu, "Control and analysis of DFIG-based wind turbines in a series compensated network for SSR damping," in *Proc. IEEE PES Gen. Meeting*, Jul. 2010, pp. 1–6.

[52] S. Tohidi, H. Oraee, M. R. Zolghadri, S. Shao, and P. Tavner, "Analysis and enhancement of low-voltage ride-through capability of brushless doubly fed induction generator," *IEEE Trans. Ind. Electron.*, vol. 60, no. 3, pp. 1146–1155, Mar. 2013.

[53] P. C. Krause, O. Wasynczuk, S. D. Sudhoff, and S. Pekarek, *Analysis of Electric Machinery and Drive Systems*, vol. 2. Hoboken, NJ, USA: Wiley, 2002.

[54] S. Skogestad and I. Postlethwaite, "Multivariate feedback control," in *Analysis and Design*. Hoboken, NJ, USA: Wiley, 1996.

[55] S. R. Jayakrishnan, E. P. Cheriyan, and T. K. Sindhu, "Identification and analysis of subsynchronous oscillations in DFIG based wind power plants," in *Proc. IEEE Region Conf. (TENCON)*, Nov. 2016, pp. 850–853.

[56] P. Kundur, N. J. Balu, and M. G. Lauby, *Power System Stability and Control*, vol. 7. New York, NY, USA: McGraw-Hill, 1994.

[57] D. Zhang, Y. Wang, J. Hu, S. Ma, Q. He, and Q. Guo, "Impacts of PLL on the DFIG-based WTG's electromechanical response under transient conditions: Analysis and modeling," *CSEE J. Power Energy Syst.*, vol. 2, no. 2, pp. 30–39, Jun. 2016.

[58] J. Liu, W. Yao, J. Wen, J. Fang, L. Jiang, H. He, and S. Cheng, "Impact of power grid strength and PLL parameters on stability of grid-connected DFIG wind farm," *IEEE Trans. Sustain. Energy*, vol. 11, no. 1, pp. 545–557, Jan. 2020.

[59] L. Fan and Z. Miao, "An explanation of oscillations due to wind power plants weak grid interconnection," *IEEE Trans. Sustain. Energy*, vol. 9, no. 1, pp. 488–490, Jan. 2018.

S. R. JAYAKRISHNAN was born in Kerala, India. He received the B.Tech. degree in electrical and electronics engineering from Kerala University, India, in 2011, and the M.Tech. degree in integrated power systems from the Visvesvaraya National Institute of Technology (VNIT), Nagpur, India, in 2014. He is currently pursuing the Ph.D. degree with the Department of Electrical Engineering, National Institute of Technology Calicut (NITC), Kozhikode, India. His research interests include power system analysis, electrical machines theory, and SSR.

ELIZABETH P. CHERIYAN (Senior Member, IEEE) was born in Alappuzha, India. She received the B.Tech. degree in electrical engineering from Kerala University, India, in 1996, and the M.Tech. degree in energetics from the National Institute of Technology Calicut, India, in 1998, and the Ph.D. degree from the Indian Institute of Technology, Bombay, India, in 2008. She has recently retired as a Professor with the Department of Electrical Engineering, National Institute of Technology Calicut. Her teaching and research interests include distributed generation and smart grid technologies.

T. K. SINDHU (Member, IEEE) was born in India, in 1975. She received the B.Tech. and M.Tech. degrees from the Government College of Engineering Trichur, Kerala, India, and the Ph.D. degree from IIT Chennai, India, in 2008. She is currently an Associate Professor with the Department of Electrical Engineering, National Institute of Technology Calicut, Kozhikode, India. Her current research interests include power systems, electromagnetic interference, dielectric properties of polymer nanocomposite materials, condition monitoring of power apparatus, and non-thermal plasma applications.